Binding of the Hemopressin Peptide to the Cannabinoid CB1 Receptor: Structural Insights

ARTICLE *in* BIOCHEMISTRY · NOVEMBER 2010

Impact Factor: 3.02 · DOI: 10.1021/bi1011833 · Source: PubMed

7 AUTHORS, INCLUDING:

Mario Scrima

Università degli Studi di Salerno

28 PUBLICATIONS **319** CITATIONS

SEE PROFILE

Manuela Grimaldi

Università degli Studi di Salerno

14 PUBLICATIONS **86** CITATIONS

SEE PROFILE

Maurizio Bifulco

Università degli Studi di Salerno

192 PUBLICATIONS **5,548** CITATIONS

SEE PROFILE

Anna Maria D'Ursi

Università degli Studi di Salerno

71 PUBLICATIONS **1,291** CITATIONS

SEE PROFILE

BIOCHEMISTRY
including biophysical chemistry & molecular biology
Article

Biochemistry **2010,** *49,* 10449–10457 10449
DOI: 10.1021/bi1011833

Binding of the Hemopressin Peptide to the Cannabinoid CB_1 Receptor: Structural Insights[†]

Mario Scrima,[‡] Sara Di Marino,[‡] Manuela Grimaldi,[‡] Antonia Mastrogiacomo,[‡] Ettore Novellino,[§] Maurizio Bifulco,[‡] and Anna Maria D'Ursi*[,‡]

[‡]*Department of Pharmaceutical Sciences, University of Salerno, I-84084 Fisciano, Italy, and* [§]*Department of Pharmaceutical and Toxicological Chemistry, University of Naples Federico II, Naples, Italy*

Received July 27, 2010; Revised Manuscript Received October 13, 2010

ABSTRACT: Hemopressin, a bioactive nonapeptide derived from the α1 chain of hemoglobin, was recently shown to possess selective antagonist activity at the cannabinoid CB_1 receptor [Heimann, A. S., et al. (2007) *Proc. Natl. Acad. Sci. U.S.A. 104*, 20588−20593]. CB_1 receptor antagonists have been extensively studied for their possible therapeutic use in the treatment of obesity, drug abuse, and heroin addiction. In particular, many compounds acting as CB_1 receptor antagonists have been synthesized and subjected to experiments as possible anti-obesity drugs, but their therapeutic application is still complicated by important side effects. Using circular dichroism and nuclear magnetic resonance spectroscopy, this work reports the conformational analysis of hemopressin and its truncated, biologically active fragment hemopressin(1−6). The binding modes of both hemopressin and hemopressin(1−6) are investigated by molecular docking calculations. Our conformational data indicate that regular turn structures in the central portion of hemopressin and hemopressin(1−6) are critical for an effective interaction with the receptor. The results of molecular docking calculations, indicating similarities and differences in comparison to the most accepted CB_1 pharmacophore model, suggest the possibility of new chemical scaffolds for the design of new CB_1 antagonist lead compounds.

The endogenous signaling system known as the ECS[1] comprises cannabinoid receptors and endocannabinoids, the enzymes for their synthesis and inactivation, and molecular targets for endocannabinoids (*2*). The ECS is involved in a broad range of functions and has been implicated in a growing number of physiopathological conditions at both central and peripheral levels (*3*). The ECS controls appetite, food intake, energy balance, and metabolic functions (*4*). In addition, the ECS system is involved in neuroprotection (*5*−*7*), the modulation of nociception (*8*), and immune and inflammatory responses (*9*−*11*) and also influences intracellular events that control the proliferation of numerous types of cancer cells, thereby producing antitumor effects (*12*). Many (endo)cannabinoid-like compounds derived from the psychoactive component Δ^9-THC of *Cannabis sativa* have been developed and used as pharmacological tools, showing utility as appetite stimulants, antiemetics, analgesics, antiglaucoma agents (*13*, *14*), and tumor growth inhibitors (*15*), as well as in the treatment of neurodegenerative disorders such as multiple sclerosis (*16*, *17*).

To date, two different cannabinoid receptors, CB_1 and CB_2, have been identified and cloned from mammalian tissues. Whereas CB_1 is preferentially expressed in the CNS (*18*), CB_2 has been described as the predominant form expressed by peripheral immune cells (*19*, *20*). Both CB_1 and CB_2 genes encode a seven-transmembrane domain protein belonging to the $G_{i/o}$-protein-coupled receptor family (*19*). Endogenous ligands (endocannabinoids), the first two cannabinoid receptor antagonists identified (*5*, *6*), anandamide (AEA) and 2-AG, and other, more recently described cannabinoid receptor agonists (*21*−*23*) all exhibit variable selectivity for both CB_1 and CB_2 (*24*, *25*).

The therapeutic applications of cannabinoid receptor antagonists depend on ligand selectivity. In particular, selective CB_1 receptor antagonists have been extensively studied for their possible therapeutic use in the treatment of obesity (*26*, *27*), drug abuse (*28*), and heroin addiction (*29*). In particular, a large number of compounds have been synthesized and SAR data derived from their activity at the CB_1 receptor have allowed the definition of a general CB_1 pharmacophore model (*1*). Currently, rimonabant [SR141716, Acomplia, discovered by Sanofi-Synthélabo (now Sanofi-Aventis)] represents the end point of all experimentation. Rimonabant has been extensively

[†]This study was supported by the University of Salerno, by Sanofi-Aventis (M.B.), and by the "Associazione Educazione e Ricerca Medica Salernitana, ERMES".

*To whom correspondence should be addressed. Phone and fax: 0039-89-969748. E-mail: dursi@unisa.it.

[1]Abbreviations: 1D, one-dimensional; 2-AG, 2-arachidonoylglycerol; AEA, *N*-arachidonoylethanolamine; Δ^9-THC, Δ^9-tetrahydrocannabinol; Boc, *tert*-butyloxycarbonyl; CD, circular dichroism; CNS, central nervous system; CSI, chemical shift index; DCM, dichloromethane; DIPEA, *N*,*N*-diisopropylethylamine; DMF, *N*,*N*-dimethylformamide; DPC, dodecylphosphocholine; DQF-COSY, double-quantum-filtered correlation spectroscopy; ECS, endocannabinoid system; ESCI-MS, electrospray/chemical ionization mass spectra; Fmoc, 9-fluorenylmethyloxycarbonyl; HATU, *O*-(7-azabenzotriazol-1-yl)-1,1,3,3-tetramethyluronium hexafluorophosphate; HFA, hexafluoroacetone; HFIP, hexafluoroisopropanol; HOBt, *N*-hydroxybenzotriazole; HPLC, high-performance liquid chromatography; LGA, Lamarckian genetic algorithm; MD, molecular dynamics; NMM, *N*-methylmorpholine; NMR, nuclear magnetic resonance; NOE, nuclear Overhauser effect; NOESY, NOE spectroscopy; PDB, Protein Data Bank; Pbf, 2,2,4,6,7-pentamethyldihydrobenzofuran-5-sulfonyl; PDF, probability density function; rmsd, root-mean-square deviation; RP-HPLC, reverse phase HPLC; t_R, retention time; SAR, structure−activity relationship; SDS, sodium dodecyl sulfate; SPPS, solid phase peptide synthesis; SVRs, structurally variable regions; TBTU, 2-(1*H*-benzotriazol-1-yl)-1,1,3,3,-tetramethyluronium tetrafluoroborate; TFA, trifluoroacetic acid; TFE, trifluoroethanol; TOCSY, total correlated spectroscopy; Trt, trityl; UPLC, ultraperformance liquid chromatography.

Published on Web 11/09/2010

studied for its application as an anti-obesity drug, but its therapeutic application is still complicated by CNS side effects. Consequently, new molecules endowed with CB_1-selective antagonist activity and devoid of side effects still represent an unmet need in medicinal chemistry.

Hemopressin, a bioactive nonapeptide derived from the α1 chain of hemoglobin, was recently found to be endowed with significant CB_1 receptor-selective antagonist activity (*1*). Hemopressin (PVNFKFLSH) (*30*) was previously isolated from rat brain homogenates and is known to cause hypotension in anesthetized rats. Using an ELISA test with anti-CB_1 receptor antibodies, Heimann et al. showed that hemopressin significantly attenuates the agonist-induced increase in the level of antibody recognition, and the extent of this decrease is the same as that of SR141716 (rimonabant); moreover, hemopressin was proven to displace [^{3}H]SR141716 binding with an affinity in the subnanomolar range (EC_{50} = 0.35 nM). In experiments with different G-protein-coupled receptors, hemopressin proved to be a selective antagonist because it efficiently blocked signaling by CB_1 receptors, but not by other members of the G-protein-coupled receptor family (including the closely related CB_2 receptors). Additionally, hemopressin acted as a CB_1 receptor inverse agonist, as it was able to block the constitutive activity of these receptors to the same extent as the well-characterized antagonist rimonabant (*1*). Data for C-terminally truncated hemopressin fragments have shown that intact hemopressin is not essential for the expression of full antinociceptive activity; indeed, hemopressin(1−6) PVNFKF and hemopressin(1−7) PVNFKFL were as effective as hemopressin in exerting antihyperalgesic effects. However, shorter fragments (PVNFK and PVNF) were inactive (*31*).

Using CD and NMR spectroscopy, this work aims to determine the conformational analysis of hemopressin and its truncated, biologically active fragment hemopressin(1−6). The binding modes of both hemopressin and hemopressin(1−6) were investigated by molecular docking calculations.

Peptides are limited in their therapeutic use because of their chemical instability in vivo and, consequently, their unfavorable pharmacokinetic profiles. For this reason, conventional medicinal chemistry research strategies generally use biologically relevant forms to produce nonpeptide compounds for therapeutic use. To be consistent with this approach, the conformational study of hemopressin, following the identification and the examination of many nonpeptide CB_1 ligands, may be considered a nonconventional medicinal chemistry research strategy. However, hemopressin, in view of its peptide nature, carries a multiplicity of chemical moieties that could potentially inspire new ideas for better defining and extending the actual CB_1 antagonist pharmacophore model.

Our CD and NMR conformational data indicate that regular turn structures in the central portion of hemopressin and hemopressin(1−6) are critical for an effective interaction with the receptor. The results of molecular docking calculations, indicating similarities and differences in comparison to the most accepted CB_1 pharmacophore model, suggest the possibility of new chemical scaffolds for the design of new CB_1 antagonist lead compounds.

EXPERIMENTAL PROCEDURES

Solid Phase Peptide Synthesis and Purification. Hemopressin (PVNFKFLSH) and hemopressin(1−6) were synthesized according to published methods using standard solid phase synthesis techniques. Protected amino acids and chemicals were purchased from Fluka (Sigma Aldrich). NR-Fmoc derivatives of amino acids were used in the coupling reactions. All lateral amino acid protections were TFA labile. Wang resin (0.6−1.0 mmol/g, 0.2 g) was treated with NR-Fmoc amino acid derivatives (4-fold excess), which were sequentially coupled to the growing peptide chain using HATU (4-fold excess) in DMF and DIPEA (8-fold excess). The coupling reaction time was 2 h. After deprotection of the last NR-Fmoc group, the peptide resin was washed with methanol and dried in vacuo to yield the protected peptide−Wang resin complex. The protected peptide was cleaved from the resin by treatment with a TFA/H_2O/phenol/ethanedithiol/thioanisole mixture (reagent K) (82.5:5:5:2.5:5, v/v) at a ratio of 10 mL to 0.5 g of resin at room temperature for 3 h. After filtration of the exhausted resin, the solvent was concentrated in vacuo and the residue was triturated with ether.

The crude peptide was purified by preparative RP-HPLC using a Jupiter [Phenomenex, Anzola Emeilia (BO), Italy] C18 column (25 cm × 4.6 cm, 5 μm, 300 Å pore size). The column was perfused at a flow rate of 1.5 mL/min with a mobile phase containing solvent A (0.1% TFA in water). A linear gradient from 30 to 45% solvent B (acetonitrile in 0.1% TFA) for 15 min was adopted for peptide elution. The pure fraction was collected to yield a white powder after lyophilization. The molecular weight of the compound was determined by mass spectral analysis.

Mass Spectral Analysis. Peptide fragments were characterized using a Finnigan LCQ-Deca ion trap instrument equipped with an electrospray source (LCQ Deca Finnigan, San Jose, CA). The samples were directly infused into the ESI source using a syringe pump set at a flow rate of 5 μL/min. Data were analyzed with Xcalibur.

Sample Preparation for CD and NMR Analysis. To conduct CD and NMR experiments in a water solution, we added hemopressin and hemopressin(1−6) to an aqueous solution (pH 5.4, 25 mM phosphate buffer). This yielded final concentrations of 0.15 mM (CD experiments) and 1.5 mM (NMR experiments). For NMR samples, a H_2O/D_2O mixture (90:10, v/v) was used.

The samples for CD and NMR experiments in mixed micelles of DPC and SDS (90:10 molar ratio) were prepared by dissolving hemopressin and hemopressin(1−6) (0.15 mM for CD experiments and 1.5 mM for NMR experiments) in a DPC/SDS water mixture. The DPC concentration used was 27 mM (27 times higher than the DPC critical micelle concentration) (*32*), and the molar DPC:SDS ratio was 90:10 (27 mM:3 mM) to reproduce the partial (2−3%) negative charge present in the typical membrane of eukaryotic cells (*33*). The final pH was adjusted to 5.4 using 20 mM phosphate buffer. For NMR experiments, SDS-d_{25} and DPC-d_{38} were used.

CD Analysis. All CD spectra were recorded using a JASCO J810 spectropolarimeter at room temperature with a cell path length of 1 mm. CD spectra were recorded at 25 °C using a measurement range from 260 to 190 nm, a 1 nm bandwidth, four accumulations, and a 10 nm/min scanning speed. Spectra were corrected for solvent contribution.

For an estimation of secondary structure content, CD spectra were analyzed using the SELCONN algorithm from the DICHROWEB website (*34*, *35*).

NMR Analysis. NMR spectra were recorded using a Bruker DRX-600 spectrometer at 300 K. 1D NMR spectra were recorded in the Fourier mode with quadrature detection. The water signal was suppressed by low-power selective irradiation in the

homogated mode. DQF-COSY, TOCSY, and NOESY (*36*−*38*) experiments were conducted in the phase-sensitive mode using quadrature detection in ω_1 via time-proportional phase increases of the initial pulse. Data block sizes were 2048 addresses in t_2 and 512 equidistant t_1 values. Prior to Fourier transformation, the time domain data matrices were multiplied by shifted $\sin^2$ functions in both dimensions. A mixing time of 70 ms was used for the TOCSY experiments. NOESY experiments were conducted with mixing times in the range of 100−300 ms. Qualitative and quantitative analyses of DQF-COSY, TOCSY, and NOESY spectra were achieved using SPARKY (*39*). To quantitatively estimate NOESY data, NOE buildup curves were produced (see the Supporting Information). Accordingly, the 300 ms NOESY spectra were chosen for the quantitative analysis.

NMR Structure Calculations. Peak volumes were translated into upper distance bounds with the CALIBA routine from the DYANA software package (*40*). The requisite pseudoatom corrections were applied for nonstereospecifically assigned protons at prochiral centers and for the methyl group. After redundant and duplicated constraints had been discarded, the final list of experimental constraints was used to generate an ensemble of 100 structures by the standard DYANA protocol of simulated annealing in torsion angle space implemented (using 6000 steps). No dihedral angle or hydrogen bond restraints were applied. The best 20 structures that had low target function values (0.83−1.19) and small residual violations (maximum violation of 0.38 Å) were refined by in vacuo minimization in the AMBER 1991 force field using the SANDER program of the AMBER 5.0 suite (*41*, *42*). To mimic the effect of solvent screening, all net charges were reduced to 20% of their real values. Moreover, a distance-dependent dielectric constant ($\varepsilon = r$) was used. The cutoff for nonbonded interactions was 12 Å. NMR-derived upper bounds were imposed as semiparabolic penalty functions, with force constants of 16 kcal mol^{-1} $Å^{-2}$. The function was shifted to be linear when the violation exceeded 0.5 Å. The best 10 structures after minimization had AMBER energies ranging from −441.4 to −391.1 kcal/mol. Final structures were analyzed using Insight 98.0 (Molecular Simulations, San Diego, CA).

Homology Modeling of the CB_1 Receptor in Its Inactive State. The sequential alignment of rhodopsin and the cannabinoid receptor CB_1 was performed using the sequence alignment program CLUSTALW (*43*) followed by a manual adjustment according to Salo et al. (*44*). From the best alignment, three-dimensional (3D) models containing all non-hydrogen atoms were obtained automatically using the method implemented in MODELER (*45*−*47*). On the basis of the sequence alignments, MODELER extracts a large number of spatial restraints from the template structures and builds a molecular model of the query protein. The restraints are generally obtained by assuming that the corresponding distances and angles between aligned residues in the template and the target structures are similar. To generate the inactive state model, CB_1 receptor Lys192−Asp366 and Arg214−Asp338 salt bridges were added as restraints (*48*, *49*).

A 3D model was obtained by optimization of molecular PDF. Of the 30 models generated with MODELER, the one corresponding to the lowest value of the PDF and fewest restraints violations was used for further analysis.

The SVRs were built as loops with the standard procedure in MODELER and afterward were refined; 20-loop models were generated for each 3D model obtained. Final models were minimized using the steepest descent and conjugate gradient methods (*50*) (as implemented in Macromodel version 8.1, Schrödinger, Inc., Portland, OR). All atom force field and Kollman charges were designed to avoid possible unfavored contacts. After refinement, the stereochemical quality of the resulting protein structure was tested with PROCHECK (*51*).

Docking Studies. AutoDock Vina version 1.0 (*52*) and AutoDock version 4.2 (*53*) in combination with the LGA were used for all docking calculations.

The starting conformations for docking studies of hemopressin and hemopressin(1−6) were obtained by our NMR studies (see Experimental Procedures); rimonabant coordinates were downloaded from the 3DCHEM website (http://www.3dchem.com/molecules.asp?ID = 348#).

For both docked ligands, only side chain bonds were treated as active torsional bonds, limiting the conformational space using NOE constraints. Lys192, Trp255, Tyr275, and Asp366, known to be crucial at the binding site (*48*, *49*), were treated as flexible to emphasize the dynamic properties of the binding site. To rapidly confirm the potential binding mode and the correct accommodation of the ligands in the binding site, preliminary docking studies were conducted using AutoDock Vina version 1.0 (data not shown) using an energy range of 10 and an exhaustiveness parameter of 8. For all docking calculations, a grid box size of 22 × 18 × 28 points (spacing between the grid points of 1 Å) was used, centered on the center of the target-binding site.

For an exhaustive exploration of conformational space, AutoDock version 4.2 was used; 20 docking calculations consisting of 256 runs were performed, yielding 5120 structures. An initial population of 450 randomly placed individuals, a maximum number of 5×10^6 energy evaluations, and a maximum number of 4×10^6 generations were taken into account. The mutation and crossover rates used were 0.02 and 0.80, respectively. The local search probability was 0.26. For all docking calculations, a grid box size of 64 × 47 × 90 points (spacing between the grids points of 0.402 Å) was used, centered on the center of the target-binding site.

Docking calculations was performed with recompiled AutoDock version 4.2 and obtained by editing and recompiling the source code to overcome the standard binary limitations as the maximum number of torsionals. The resulting data, differing by less than 3.5 Å in positional rmsd, were clustered together and represented by the result with the most favorable free energy of binding. All 3D models were depicted using Python and Mgl Tools 1.5.4 and the VMD molecular visualization program (*54*, *55*). Molecular surfaces were rendered using the maximal speed molecular surface (*56*).

RESULTS

CD Spectroscopy. The conformational preferences of hemopressin and hemopressin(1−6) were preliminarily screened by CD spectroscopy. Figure 1 shows the CD spectra of hemopressin and hemopressin(1−6) recorded in water and in 90:10 (molar ratio) DPC/SDS mixtures. The CD spectrum recorded in aqueous solution at pH 5.4 indicates the prevalence of disordered structures in this medium. The CD spectra of both hemopressin and hemopressin(1−6) acquired in DPC/SDS mixed micelles showed a negative ellipticity value at 218 nm. The quantitative evaluation of the CD curves mentioned above, which was performed using the DICHROWEB (*34*, *35*) interactive website (SELCONN algorithm), indicated that hemopressin and hemopressin(1−6) in a water solution assume random coil

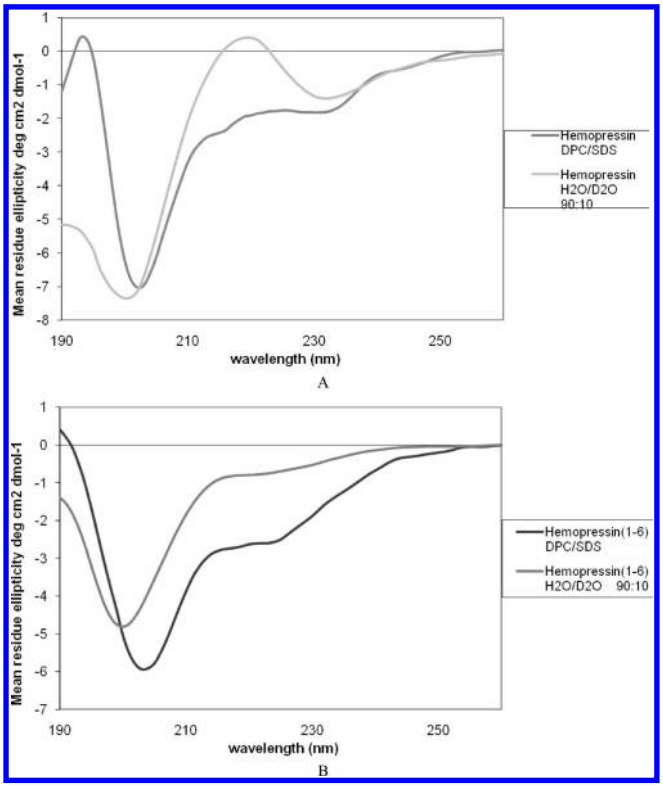

FIGURE 1: CD spectra of hemopressin (A) and hemopressin(1−6) (B) recorded in water and in DPC/SDS mixtures (90:10 molar ratio).

conformations with minimal amounts of turn and strand structures. In mixed DPC/SDS micelles, hemopressin and hemopressin(1−6) prevalently assume α-helical and β-turn, with small amounts of random coil conformations. In particular, hemopressin is present as 27% helical, 40% β-turn, 13% β-strand, and 20% random coil conformations, whereas hemopressin(1−6) assumes 60% helical, 30% β-turn, and 10% random coil conformations.

NMR Spectroscopy. (*i*) *Chemical Shift Analysis*. An entire set of 1D and 2D proton spectra of hemopressin and hemopressin(1−6) were recorded in water and in DPC/SDS (90:10 molar ratio) mixed micelles. To determine the absence of self-aggregation, spectra were recorded in the peptide concentration range of 0.5−15 mM. No significant changes were observed in the distribution and shape of ^{1}H resonances, indicating that no aggregation phenomena occurred in this concentration range.

COSY (*36*, *57*), TOCSY (*37*), and NOESY (*38*) 2D spectra were recorded, and complete assignments of the proton spectra of hemopressin and hemopressin(1−6) both in water and in micelle solutions (see the Supporting Information) were achieved by the standard Wüthrich procedure (*58*). Analysis of 2D spectra was performed using SPARKY (*39*). Few and weak NOE effects were observed in the NOESY spectra recorded in water solutions, confirming the CD data that showed that both hemopressin and its shorter analogue are disordered in water solutions.

It is well-known that the values of CHα proton chemical shifts are diagnostic of specific secondary structures. According to the CSI (*59*), groups of four (not necessarily consecutive) CHα atoms showing <0.1 ppm upfield shifted values, as compared to random coil values, are diagnostic of turn−helix conformations. Regions characterized by nonconsecutive CHα values that are close or low-field shifted compared to the CHα random coil

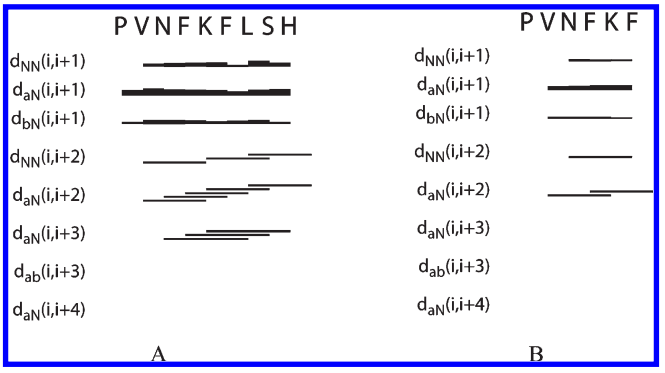

FIGURE 2: NOE connectivities collected in the NOESY spectra of hemopressin (A) and hemopressin(1−6) (B) in DPC/SDS (90:10 molar ratio) micelle solutions.

values are diagnostic of coil conformations (*59*). CHα proton chemical shift differences of hemopressin and hemopressin(1−6) in water indicate values close to those reported for random coil peptides (*58*), thus confirming the presence of both the peptides in random coil conformations. In contrast, the negative CHα chemical shift differences for hemopressin and hemopressin(1−6) in DPC/SDS micelles (90:10 molar ratio), particularly in the Phe4−Leu7 segment, indicated the preponderance in this segment of turn−helix conformations (data not shown).

(*ii*) *NMR Structure Calculation*. Figure 2 summarizes the NOE connectivities observed in the NOESY spectra of hemopressin and hemopressin(1−6) in DPC/SDS mixed micelles. Hemopressin exhibited a regular pattern of NOE connectivities, consisting of sequential NH−NH(*i*,*i*+1), CHα−NH(*i*,*i*+3), and CHα−NH(*i*,*i*+2) effects along the full sequence. On the other hand, the hemopressin(1−6) NOE pattern was characterized by regular NH−NH(*i*,*i*+1) effects in the Asn3−Ser8 segment, CHα−NH(*i*,*i*+2) correlations involving residues Val2−Phe4 and Phe4−Phe6, and NH−NH(*i*,*i*+2) effects involving residues Asn3−Lys5.

The structural calculations of hemopressin and hemopressin(1−6) in DPC/SDS mixed micelles were performed using DYANA based on NOE data. These data were transformed into interprotonic distances and imposed as restraints in the calculation. Among 50 calculated structures, the resulting best 20 were selected according to the lowest values of their target functions. These structures were subjected to further minimization procedures with the SANDER module of AMBER version 5.0 (*41*, *42*), using DYANA-derived restraints.

Figure 3 shows NMR structure bundles of hemopressin and hemopressin(1−6) in DPC/SDS micelles. Statistical information for the structural ensemble of hemopressin and hemopressin(1−6) in DPC/SDS micelles is reported in the Supporting Information. Analysis of hemopressin structure bundles according to the PROMOTIF procedure (*60*) using Kabsh and Sanders parameters points to the presence of regular type I β-turn structures for residues Phe4−Leu7, Lys5−Ser8, and Phe6−His9. Hydrogen bonds between C═O (Phe4) and HN (Leu7) as well as between C═O (Phe6) and HN (His9) stabilize the β-turn structures. Analysis of hemopressin(1−6) structure bundles following the procedure reported for hemopressin indicates that this shorter fragment assumes γ-turn structures centered on residues Phe4−Phe6.

Homology Modeling Results. The homology modeling process consists of several alignment steps essential for producing the correct sequence alignment of a template sequence [PDB entry 1GZM (*61*)] with the homologous sequence of the target protein.

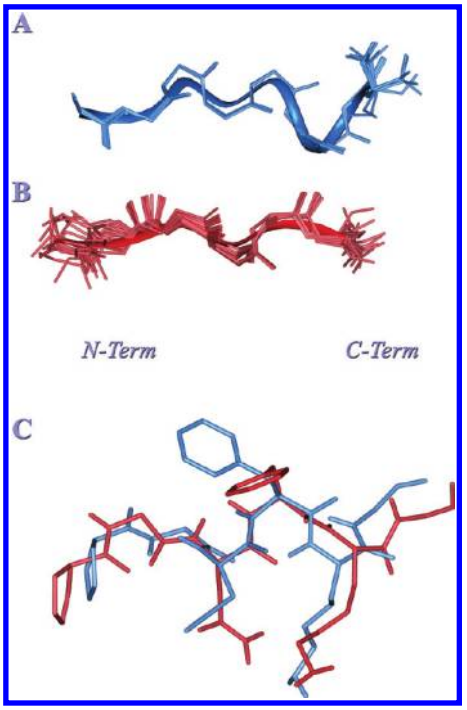

FIGURE 3: NMR structure bundles of hemopressin (sky blue, A) and hemopressin(1−6) (red, B) in DPC/SDS micelles (90:10 molar ratio). (C) Superimposition of representative NMR structures of hemopressin (sky blue) and hemopressin(1−6) (red).

The CB_1 receptor is 21% identical with visual rhodopsin [PDB entry 1GZM (*61*)]. On the basis of previously performed alignment studies (*44*, *62*), we built a molecular model of the CB_1 receptor using MODELER (*45*−*47*). According to the MODELER procedure, the model was calculated using spatial restraints derived from the template structures and selected by assuming that distances and angles of aligned residues were similar. The E2 loop was not considered to focus solely on the cannabinoid binding site within the helix bundle.

To generate the inactive state receptor model, salt bridges involving Lys192−Asp366 (*48*) and Arg214−Asp338 were imposed as restraints (*49*). To evaluate the quality of the final model (*63*), the presence of these salt bridges, the gauche+ $\chi 1$ configuration of TRP356, and the aromatic cluster including Trp356, Phe200, and Tyr275 (*49*) was verified (Figure 4).

The stereochemical quality of the CB_1 model was assessed using PROCHECK (*51*). The final results (see Figure 5) showed 94.8% of residues in the most favored regions, 4% in additional allowed regions, 0.4% in generously allowed regions, and 0.8% in disallowed regions; the residues in disallowed regions were not located in the binding pocket. The stereochemical analysis did not consider the N-terminal residues 1−110, C-terminal residues 421−472, and the E2 loop.

Molecular Docking Results. To study the binding mode of hemopressin and hemopressin(1−6) at the CB_1 receptor-binding site, molecular docking studies with selective receptor flexibility were performed. The molecular docking of rimonabant was conducted to have an internal CB_1 binding mode reference. Rimonabant and several other analogues have been shown to act as inverse agonists on a constitutively active CB_1 receptor (*64*−*66*). Structural and biochemical studies (*48*, *61*, *62*) have shown key interactions between rimonabant and its analogues at the CB_1 binding site.

Table 1A summarizes the most significant interactions occurring between rimonabant and the CB_1 binding site resulting from our molecular docking calculations. Analysis of the data shows that these interactions are consistent with those reported in the quoted studies (*48*, *49*, *64*−*66*). In particular, the carboxamide oxygen of rimonabant formed hydrogen bonds with Lys192 Nζ (Figure 6) and Asp366 C═O. This hydrogen bond exerts a stabilizing effect on the Lys192−Asp366 salt bridge of the intracellular end of transmembrane helices 3 and 6. The existence of this specific salt bridge was induced by a pronounced kink at the level of Pro358 in transmembrane helix 6; this kink is present in the inactive R state of the receptor but absent in the active R* state that is stabilized by receptor agonist binding (*64*). The 2,4-dichlorophenyl and 4-chlorophenyl rings of rimonabant produce aromatic stacking interactions with Trp279/Phe200/Tyr275 and Trp356 (*48*, *49*). The lipophilic piperidinyl moiety was involved in hydrophobic interactions with Val196, Met363, Met384, Leu387, and Phe379 (Figure 6).

Molecular docking calculations of hemopressin at the CB_1 binding site were conducted starting from the low-energy hemopressin NMR structure. Table 1B summarizes the most significant interactions involving hemopressin with the CB_1 binding pocket. The binding of hemopressin at the CB_1 binding site was stabilized by essential hydrogen bonds between Asn3 C═O (hemopressin) and Lys192 Nζ (CB_1 receptor) and between Lys5 Nζ (hemopressin) and Asp366 C═O (CB_1 receptor) (Figure 7). The phenyl rings of residues Phe4 and Phe6 of hemopressin were involved in hydrophobic interactions with CB_1 receptor residues Phe189, Trp255, and Leu190, and Phe368, and Met363, respectively. Pro1 and Val2 hemopressin N-terminal residues were involved in van der Waals hydrophobic interactions with Phe180, His181, and Ile375. Ser8 and His9 hemopressin C-terminal residues interacted with residues neighboring those of the binding site.

Table 1C summarizes intermolecular hydrogen bonds and hydrophobic contacts between hemopressin(1−6) and the CB_1 receptor. In a way analogous to that of hemopressin, interaction of hemopressin(1−6) at the binding site was stabilized by hydrogen bonds between Asn3 C═O [hemopressin(1−6)−Lys192 Nζ (CB_1 receptor)] and Lys5 Nζ [hemopressin(1−6)−Asp366 C═O (CB_1 receptor)] (Figure 8). The phenyl rings of Phe4 and Phe6 were involved in hydrophobic contacts with Leu193 and Phe189, and Phe368, Val367, and Gly369, respectively. Pro1 and Val2 of hemopressin(1−6) participated in the binding thorough van der Waals interactions with Phe177, Phe180, His181, and Arg182.

DISCUSSION

A great deal of experimentation has attempted to identify an optimal CB_1 ligand to be employed in therapy for drug addiction and obesity control. Several compounds have been extensively investigated as promising candidates for therapeutic applications, but many of them are not suitable for clinical use because of toxicity and related side effects. Accordingly, there is an unmet need for new CB_1 ligands to be used as new lead compounds for the CB_1 receptor. In this work, we have reported an extensive structural study of hemopressin and its shorter active fragment, hemopressin(1−6). The identification of the conformational features of hemopressin and hemopressin(1−6) and the discovery of their binding modes at the CB_1 binding site may help in the identification of new CB_1 antagonist lead compounds to be developed for therapeutic employment.

We studied the structural features of hemopressin in a membrane-mimicking environment composed of an SDS micelle solution. For peptides acting as ligands of membrane receptors,

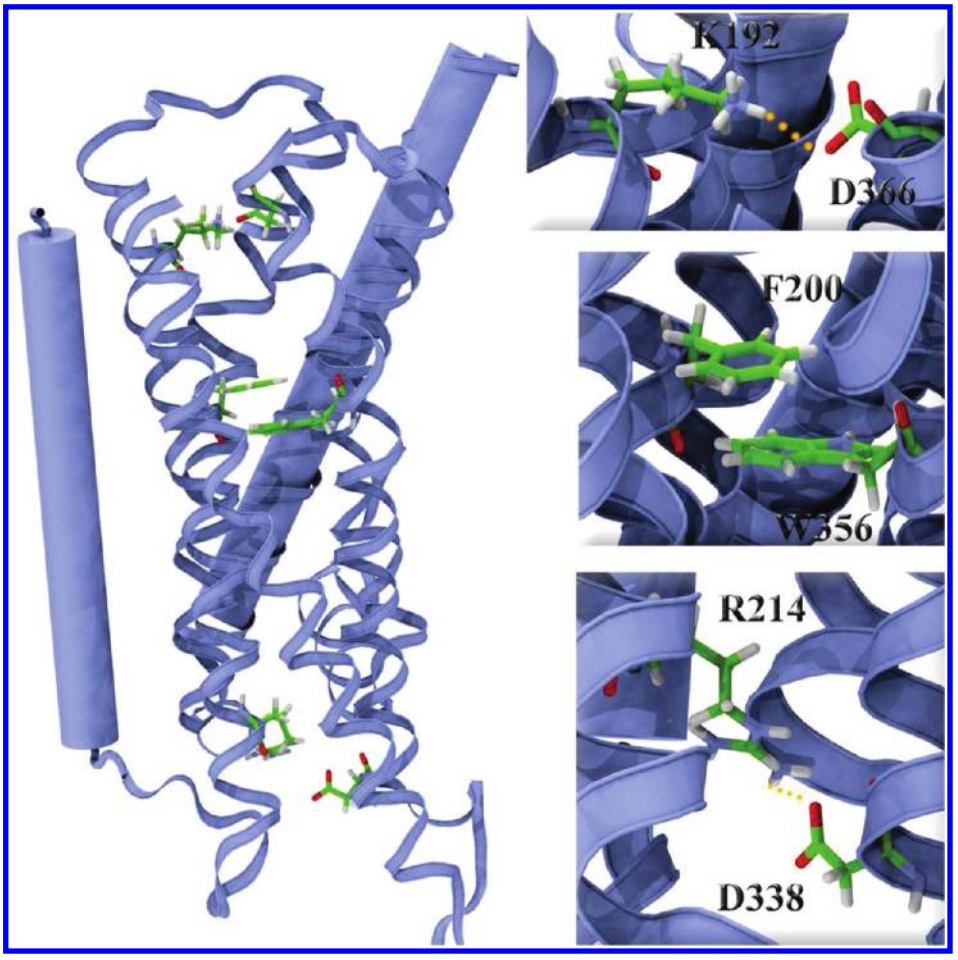

FIGURE 4: Molecular model of the CB_1 receptor in the inactive state as predicted by homology modeling. The protein backbone is shown as a sky blue ribbon and tube. The critical residues that characterize the CB_1 inactive state are shown as sticks and colored by atom type. On the right, residues crucial to stabilization of the receptor three-dimensional structure are shown.

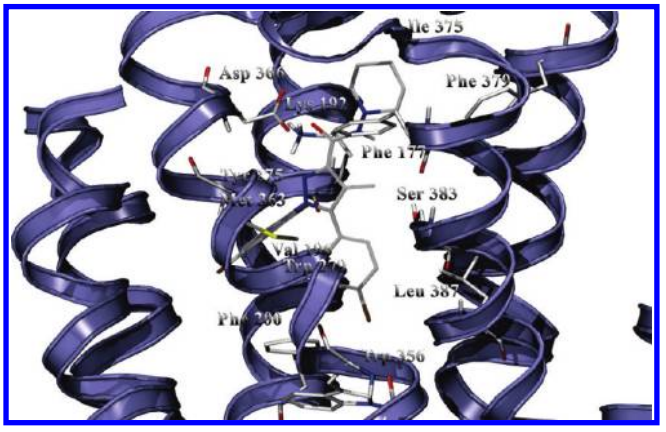

FIGURE 5: (A) Binding conformation of rimonabant in the CB_1 receptor. Rimonabant is colored by atom type. The protein molecular surface is colored gray. (B) Ribbon representation of the CB_1 receptor. The amino acid residues involved in the binding with rimonabant are shown as sticks and colored by atom type.

Table 1: H-Bond Interactions Involving the CB_1 Receptor and CB_1 Antagonists Rimonabant, Hemopressin, and Hemopressin(1−6)

ligand	protein	length (Å)	acceptor−H−donor angle (deg)
	(A) Rimonabant		
carboxamide oxygen	Lys192 Nζ	2.82	145
carboxamide hydrogen	Asp366 CO	3.40	163
pyrazole nitrogen	Tyr275 OH	2.81	148
	(B) Hemopressin		
Asn3 CO	Lys192 Nζ	2.80	134.8
Lys5 Nζ	Asp366 CO	2.90	129
Lys5 CO	Asp272 NH	2.86	136.8
	(C) Hemopressin(1−6)		
Asn3 CO	Lys192 Nζ	2.83	126.85
Lys5 Nζ	Asp366 CO	2.65	123.68

the use of a membrane mimetic medium such as SDS or DPC is suggested, leading to the hypothesis of membrane-assisted mechanisms of interactions between peptides and their receptors. According to this model, the membrane surface plays a key role in facilitating the transition of the peptide from a random coil conformation adopted in the extracellular environment to a conformation that is recognized by the receptor. The increase in the local concentration of the peptide and the reduction of the degree of rotational and translational freedom of the neuropeptide are membrane-mediated events acting as determinant steps for the conformational transition of the peptide (*67*−*71*).

CD and NMR data revealed the tendency of both fragments to assume ordered secondary structures in the micelle solution. In particular, hemopressin is characterized by regular β-turn structures in the Asn3−His9 segment, whereas hemopressin(1−6) shows a regular β-turn conformation in the Asn3−Phe6 segment.

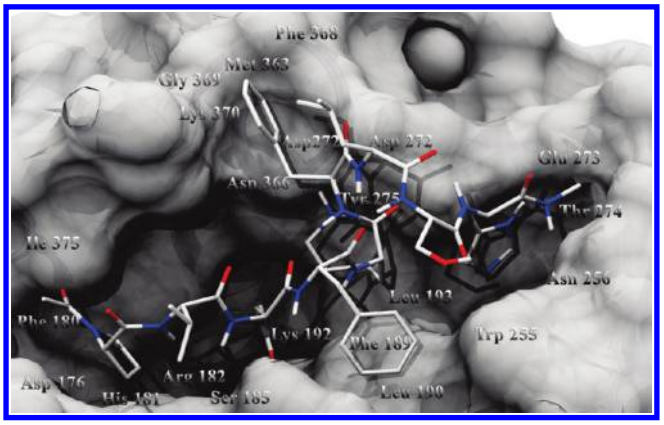

FIGURE 6: Binding conformation of hemopressin at the CB_1 receptor binding site. Hemopressin is colored by atom type. The protein molecular surface is colored light gray.

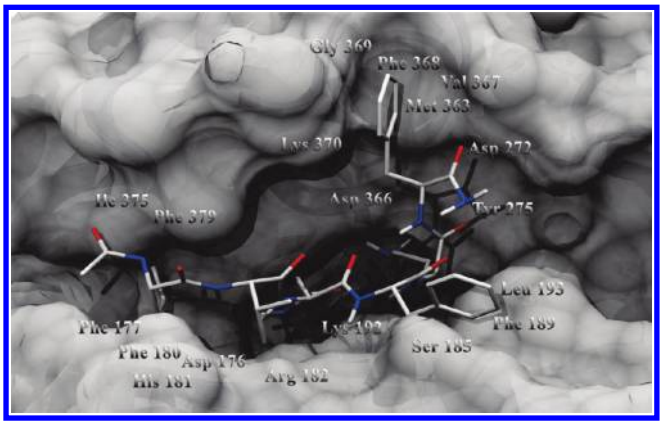

FIGURE 7: Binding conformation of hemopressin(1−6) at the CB_1 binding site. Hemopressin(1−6) is colored by atom type. The protein molecular surface is colored light gray.

Therefore, in both peptides, regular turn structures are present in the Asn3−Phe6 segment, with good overlapping of the aromatic Phe rings (rmsd = 0.1) (Figure 3C). The structural regularity of the Asn3−Phe6 segment as a common structural feature of hemopressin and hemopressin(1−6) suggests the possibility that this segment may include chemical moieties essential for interaction with the receptor.

Conformational data indicated that, excluding the Asn3−Phe6 segment, the structural regularity of the N- and C-terminal portions does not correlate with biological activity. In fact, hemopressin C-terminal residues Leu7−His9, which do not appear to be essential for biological activity (*31*), assumed regular β-turn structures, whereas Pro1 and Val2, which proved to be important for CB_1 antagonist activity, preferentially assume flexible conformations.

To investigate the binding mode of hemopressin and hemopressin(1−6) at the CB_1 binding site, we performed molecular docking calculations of both peptides with the CB_1 receptor, starting from their low-energy NMR structures. A general overview of hemopressin and hemopressin(1−6) binding poses shows that hemopressin(1−6), characterized by a smaller molecular surface compared to that of hemopressin, has the ideal dimensions to fit the CB_1 binding pocket. Because of their larger molecular size, the C-terminal residues of hemopressin are confined in a region external to the binding site.

Energy values and binding and docking constants show that the binding of hemopressin and hemopressin(1−6) at the CB_1 receptor was significantly stabilized by H-bonds involving residues Asn3 and Lys5 with Lys192 and Asp366, respectively, of the CB_1 receptor. Moreover, hemopressin and hemopressin(1−6) interacted with the CB_1 binding site through hydrophobic interaction involving Phe4 and Phe6 aromatic residues as well as Pro1 and Val2 N-terminal residues. In particular, for both peptides, Phe4 was involved in van der Waals contacts with Phe89, Ser185, Arg182, and Trp255 of the CB_1 receptor; Phe6 was involved in van der Waals contacts with Gly369, Asp272, Phe368, and Lys370 of the CB_1 receptor. In hemopressin and hemopressin(1−6), Pro1 interacted with Phe180, Ile375, Phe177, and His181 and Val2 interacted with Arg182 and His181.

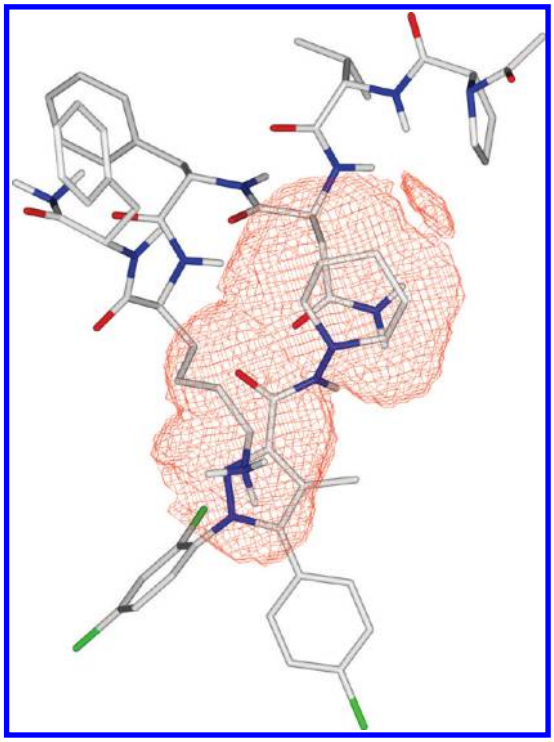

FIGURE 8: Superimposition of binding poses of hemopressin(1−6) and rimonabant. The van der Waals volume intersection of rimonabant and hemopressin(1−6) binding poses is colored red.

As previously mentioned, to validate the binding site model, we performed docking calculations of the well-studied CB_1 antagonist rimonabant. Via comparison of the binding modes of hemopressin peptides with that reported for rimonabant, the following considerations were suggested.

(i) The hydrogen bond involving Lys192 and Asp366 of the CB_1 binding site is an essential interaction common to hemopressin and rimonabant. This interaction is crucial for the stabilization of the inactive state of the receptor and thus provides a structural basis to explain the activity of hemopressin peptides as inverse agonists.

(ii) Hemopressin and hemopressin(1−6) N-terminal residues interact with a region of the CB_1 binding pocket that was also reached by the rimonabant piperidyl ring (Figure 8). The involvement of hemopressin N-terminal residues in binding with the receptor provides a structural basis for explaining the biological data on the importance of N-terminal residues for hemopressin CB_1 antagonist activity.

(iii) Phe rings of hemopressin peptides are located in a different region within the CB_1 binding site as compared to the region reached by rimonabant aromatic rings. Rimonabant, characterized by a significantly smaller molecular size in comparison to

hemopressin peptides, penetrates a deep cavity within the CB_1 binding pocket with its aromatic rings (Figure 5); this region cannot be accessed by hemopressin and hemopressin(1−6), whose Phe rings are confined in a more external CB_1 binding site region (Figures 6 and 7).

Taken altogether, our data show that the pharmacophore present in rimonabant can be only partially recognized in hemopressin peptides. In particular, the carboxamide moiety and pyrazole ring of rimonabant may correspond to Asn3 and Lys5 of the hemopressin peptides, which are involved in a hydrogen bond with CB_1 receptor residues Lys192 and Asp366. The piperidyl ring of rimonabant may correspond to the N-terminal residues of hemopressin (Figure 8).

The dichlorophenyl ring and clorophenyl group of rimonabant, which may correspond to the aromatic rings of Phe4 and Phe6, interact with different regions of the CB_1 binding site because of the different molecular surfaces of the peptides as compared to rimonabant. Interestingly, biological data show that in spite of these different interaction sites, the CB_1 antagonist activity of hemopressin is preserved. The comparison between human and rat hemopressin sequences shows that Phe6 in human hemopressin is replaced with a Leu residue; an increasing amount of biological data indicates that human hemopressin is as biologically active as rat hemopressin (*72*). As a result, the role of the aromatic rings in the CB_1 pharmacophore model and the significance of the region contacted by aromatic rings within the receptor are questioned. Accordingly, a revision of the CB_1 pharmacophore model may be necessary, with particular attention to the region within the CB_1 binding pocket explored by hemopressin Phe rings. We are hopeful this revisiting of the pharmacophore model will facilitate the identification of novel CB_1 receptor antagonists that lack the psychoactive side effects of conventional cannabinoid-derived compounds and are potentially useful for the treatment of disorders involving the ECS.

SUPPORTING INFORMATION AVAILABLE

NMR data, including proton chemical shifts, NOE buildup curves, NMR structural statistics, NOESY spectra, Ramachandran plots, and ligand−receptor short distances. This material is available free of charge via the Internet at http://pubs.acs.org.

REFERENCES

1. Heimann, A. S., Gomes, I., Dale, C. S., Pagano, R. L., Gupta, A., de Souza, L. L., Luchessi, A. D., Castro, L. M., Giorgi, R., Rioli, V., Ferro, E. S., and Devi, L. A. (2007) Hemopressin is an inverse agonist of CB1 cannabinoid receptors. *Proc. Natl. Acad. Sci. U.S.A. 104*, 20588–20593.
2. De Petrocellis, L., Cascio, M. G., and Di Marzo, V. (2004) The endocannabinoid system: A general view and latest additions. *Br. J. Pharmacol. 141*, 765–774.
3. Cota, D., and Woods, S. C. (2005) The role of the endocannabinoid system in the regulation of energy homeostasis. *Curr. Opin. Endocrinol. Diabetes 12*, 338–351.
4. Pagotto, U., Marsicano, G., Cota, D., Lutz, B., and Pasquali, R. (2006) The emerging role of the endocannabinoid system in endocrine regulation and energy balance. *Endocr. Rev. 27*, 73–100.
5. Panikashvili, D., Simeonidou, C., Ben-Shabat, S., Hanus, L., Breuer, A., Mechoulam, R., and Shohami, E. (2001) An endogenous cannabinoid (2-AG) is neuroprotective after brain injury. *Nature 413*, 527–531.
6. Marsicano, G., Goodenough, S., Monory, K., Hermann, H., Eder, M., Cannich, A., Azad, S. C., Cascio, M. G., Gutierrez, S. O., van der Stelt, M., Lopez-Rodriguez, M. L., Casanova, E., Schutz, G., Zieglgansberger, W., Di Marzo, V., Behl, C., and Lutz, B. (2003) CB1 cannabinoid receptors and on-demand defense against excitotoxicity. *Science 302*, 84–88.
7. Panikashvili, D., Mechoulam, R., Beni, S. M., Alexandrovich, A., and Shohami, E. (2005) CB1 cannabinoid receptors are involved in neuroprotection via NF-κB inhibition. *J. Cereb. Blood Flow Metab. 25*, 477–484.
8. Cravatt, B. F., and Lichtman, A. H. (2004) The endogenous cannabinoid system and its role in nociceptive behavior. *J. Neurobiol. 61*, 149–160.
9. Walter, L., Franklin, A., Witting, A., Wade, C., Xie, Y., Kunos, G., Mackie, K., and Stella, N. (2003) Nonpsychotropic cannabinoid receptors regulate microglial cell migration. *J. Neurosci. 23*, 1398–1405.
10. Klein, T. W., Newton, C., Larsen, K., Lu, L., Perkins, I., Nong, L., and Friedman, H. (2003) The cannabinoid system and immune modulation. *J. Leukocyte Biol. 74*, 486–496.
11. Massa, F., Marsicano, G., Hermann, H., Cannich, A., Monory, K., Cravatt, B. F., Ferri, G. L., Sibaev, A., Storr, M., and Lutz, B. (2004) The endogenous cannabinoid system protects against colonic inflammation. *J. Clin. Invest. 113*, 1202–1209.
12. Bifulco, M., Malfitano, A. M., Pisanti, S., and Laezza, C. (2008) Endocannabinoids in endocrine and related tumours. *Endocr.-Relat. Cancer 15*, 391–408.
13. Croxford, J. (2003) Therapeutic potential of cannabinoids in CNS disease. *CNS Drugs 17*, 179–202.
14. Drysdale, A., and Platt, B. (2003) Cannabinoids: Mechanisms and therapeutic applications in the CNS. *Curr. Med. Chem. 10*, 2719–2732.
15. Ligresti, A., Bisogno, T., Matias, I., De Petrocellis, L., Cascio, M., Cosenza, V., D'argenio, G., Scaglione, G., Bifulco, M., and Sorrentini, I. (2003) Possible endocannabinoid control of colorectal cancer growth. *Gastroenterology 125*, 677–687.
16. Croxford, J., and Miller, S. (2004) Towards cannabis and cannabinoid treatment of multiple sclerosis. *Drugs Today 40*, 663–676.
17. Smith, P. (2004) Medicinal cannabis extracts for the treatment of multiple sclerosis. *Curr. Opin. Invest. Drugs* (*Thomson Sci.*) *5*, 727–730.
18. Matsuda, L. A., Lolait, S. J., Brownstein, M. J., Young, A. C., and Bonner, T. I. (1990) Structure of a cannabinoid receptor and functional expression of the cloned cDNA. *Nature 346*, 561–564.
19. Munro, S., Thomas, K. L., and Abu-Shaar, M. (1993) Molecular characterization of a peripheral receptor for cannabinoids. *Nature 365*, 61–65.
20. Galiegue, S., Mary, S., Marchand, J., Dussossoy, D., Carriere, D., Carayon, P., Bouaboula, M., Shire, D., Le Fur, G., and Casellas, P. (1995) Expression of central and peripheral cannabinoid receptors in human immune tissues and leukocyte subpopulations. *Eur. J. Biochem. 232*, 54–61.
21. Bisogno, T., Melck, D., Bobrov, M., Gretskaya, N. M., Bezuglov, V. V., De Petrocellis, L., and Di Marzo, V. (2000) N-Acyl-dopamines: Novel synthetic CB_1 cannabinoid-receptor ligands and inhibitors of anandamide inactivation with cannabimimetic activity in vitro and in vivo. *Biochem. J. 351* (Part 3), 817–824.
22. Huang, S. M., Bisogno, T., Trevisani, M., Al-Hayani, A., De Petrocellis, L., Fezza, F., Tognetto, M., Petros, T. J., Krey, J. F., Chu, C. J., Miller, J. D., Davies, S. N., Geppetti, P., Walker, J. M., and Di Marzo, V. (2002) An endogenous capsaicin-like substance with high potency at recombinant and native vanilloid VR1 receptors. *Proc. Natl. Acad. Sci. U.S.A. 99*, 8400–8405.
23. Porter, A. C., Sauer, J. M., Knierman, M. D., Becker, G. W., Berna, M. J., Bao, J., Nomikos, G. G., Carter, P., Bymaster, F. P., Leese, A. B., and Felder, C. C. (2002) Characterization of a novel endocannabinoid, virodhamine, with antagonist activity at the CB1 receptor. *J. Pharmacol. Exp. Ther. 301*, 1020–1024.
24. McAllister, S. D., and Glass, M. (2002) CB_1 and CB_2 receptor-mediated signalling: A focus on endocannabinoids. *Prostaglandins, Leukotrienes Essent. Fatty Acids 66*, 161–171.
25. Mechoulam, R., Panikashvili, D., and Shohami, E. (2002) Cannabinoids and brain injury: Therapeutic implications. *Trends Mol. Med. 8*, 58–61.
26. Fernandez, J., and Allison, D. (2004) Rimonabant Sanofi-Synthélabo. *Curr. Opin. Invest. Drugs* (*Thomson Sci.*) *5*, 430–435.
27. Black, S. (2004) Cannabinoid receptor antagonists and obesity. *Curr. Opin. Invest. Drugs* (*Thomson Sci.*) *5*, 389–394.
28. Hungund, B., Basavarajappa, B., Vadasz, C., Kunos, G., de Fonseca, F., Colombo, G., Serra, S., Parsons, L., and Koob, G. (2006) Ethanol, endocannabinoids, and the cannabinoidergic signaling system. *Alcohol.: Clin. Exp. Res. 26*, 565–574.
29. Solinas, M., Panlilio, L., Antoniou, K., Pappas, L., and Goldberg, S. (2003) The cannabinoid CB1 antagonist N-piperidinyl-5-(4-chlorophenyl)-1-(2, 4-dichlorophenyl)-4-methylpyrazole-3-carboxamide (SR-141716A) differentially alters the reinforcing effects of

heroin under continuous reinforcement, fixed ratio, and progressive ratio schedules of drug self-administration in rats. *J. Pharmacol. Exp. Ther. 306*, 93.
30. Dale, C. S., Pagano Rde, L., and Rioli, V. (2005) Hemopressin: A novel bioactive peptide derived from the α1-chain of hemoglobin. *Mem. Inst. Oswaldo Cruz 100* (Suppl. 1), 105–106.
31. Dale, C. S., Pagano Rde, L., Rioli, V., Hyslop, S., Giorgi, R., and Ferro, E. S. (2005) Antinociceptive action of hemopressin in experimental hyperalgesia. *Peptides 26*, 431–436.
32. Pellegrini, M., and Mierke, D. F. (1999) Structural characterization of peptide hormone/receptor interactions by NMR spectroscopy. *Biopolymers 51*, 208–220.
33. Weller, K., Lauber, S., Lerch, M., Renaud, A., Merkle, H. P., and Zerbe, O. (2005) Biophysical and biological studies of end-group-modified derivatives of Pep-1. *Biochemistry 44*, 15799–15811.
34. Whitmore, L., and Wallace, B. (2004) DICHROWEB, an online server for protein secondary structure analyses from circular dichroism spectroscopic data. *Nucleic Acids Res. 32*, W668.
35. Wesson, L., and Eisenberg, D. (1992) Atomic solvation parameters applied to molecular dynamics of proteins in solution. *Protein Sci. 1*, 227–235.
36. Piantini, U., Sorensen, O., and Ernst, R. (1982) Multiple quantum filters for elucidating NMR coupling networks. *J. Am. Chem. Soc. 104*, 6800–6801.
37. Bax, A., and Davis, D. (1985) MLEV-17-based two-dimensional homonuclear magnetization transfer spectroscopy. *J. Magn. Reson. 65*, 355–360.
38. Jeener, J., Meier, B., Bachmann, P., and Ernst, R. (1979) Investigation of exchange processes by two-dimensional NMR spectroscopy. *J. Chem. Phys. 71*, 4546–4553.
39. Goddard, T., and Kneller, D. (2004) SPARKY 3, University of California, San Francisco.
40. Guntert, P., Mumenthaler, C., and Wuthrich, K. (1997) Torsion angle dynamics for NMR structure calculation with the new program DYANA. *J. Mol. Biol. 273*, 283–298.
41. Pearlman, D., Case, D., Caldwell, J., Ross, W., and Cheatham, T. (1995) AMBER, a package of computer programs for applying molecular mechanics, normal mode analysis, molecular dynamics and free energy calculations to simulate the structural and energetic properties of molecules. *Comput. Phys. Commun. 91*, 1–41.
42. Case, D., Pearlman, D., Caldwell, J., Cheatham, T., III, Ross, W., Simmerling, C., Darden, T., Merz, K., Stanton, R., and Cheng, A. (1997) AMBER 5, University of California, San Francisco.
43. Thompson, J. D., Gibson, T. J., Plewniak, F., Jeanmougin, F., and Higgins, D. G. (1997) The CLUSTAL_X windows interface: Flexible strategies for multiple sequence alignment aided by quality analysis tools. *Nucleic Acids Res. 25*, 4876–4882.
44. Salo, O. M., Lahtela-Kakkonen, M., Gynther, J., Jarvinen, T., and Poso, A. (2004) Development of a 3D model for the human cannabinoid CB1 receptor. *J. Med. Chem. 47*, 3048–3057.
45. Sali, A., and Blundell, T. L. (1993) Comparative protein modelling by satisfaction of spatial restraints. *J. Mol. Biol. 234*, 779–815.
46. Fiser, A., Do, R. K., and Sali, A. (2000) Modeling of loops in protein structures. *Protein Sci. 9*, 1753–1773.
47. Eswar, N., Webb, B., Marti-Renom, M. A., Madhusudhan, M. S., Eramian, D., Shen, M. Y., Pieper, U., and Sali, A. (2007) Comparative protein structure modeling using Modeller. *Curr. Protoc. Protein Sci.,* Chapter 2, Unit 2.9.
48. Hurst, D. P., Lynch, D. L., Barnett-Norris, J., Hyatt, S. M., Seltzman, H. H., Zhong, M., Song, Z. H., Nie, J., Lewis, D., and Reggio, P. H. (2002) N-(Piperidin-1-yl)-5-(4-chlorophenyl)-1-(2,4-dichlorophenyl)-4-methyl-1H-pyrazole-3-carboxamide (SR141716A) interaction with LYS 3.28(192) is crucial for its inverse agonism at the cannabinoid CB1 receptor. *Mol. Pharmacol. 62*, 1274–1287.
49. McAllister, S. D., Hurst, D. P., Barnett-Norris, J., Lynch, D., Reggio, P. H., and Abood, M. E. (2004) Structural mimicry in class A G protein-coupled receptor rotamer toggle switches: The importance of the F3.36(201)/W6.48(357) interaction in cannabinoid CB1 receptor activation. *J. Biol. Chem. 279*, 48024–48037.
50. Polak, E., and Ribiere, G. (1969) Note sur la convergence de directions conjugees. *Revue Francaise Informant Recherch Operationelle, Annee 16*, 35–43.
51. Laskowski, R., MacArthur, M., Moss, D., and Thornton, J. (1993) PROCHECK: A program to check the stereochemical quality of protein structures. *J. Appl. Crystallogr. 26*, 283–291.
52. Trott, O., and Olson, A. (2009) AutoDock Vina: Improving the speed and accuracy of docking with a new scoring function, efficient optimization, and multithreading. *J. Comput. Chem. 31*, 455–461.
53. Morris, G., Huey, R., Lindstrom, W., Sanner, M., Belew, R., Goodsell, D., and Olson, A. (2009) AutoDock4 and AutoDockTools4: Automated docking with selective receptor flexibility. *J. Comput. Chem. 30*, 2785–2791.
54. Humphrey, W., Dalke, A., and Schulten, K. (1996) VMD: Visual molecular dynamics. *J. Mol. Graphics 14*, 33–38.
55. Sanner, M. F. (1999) Python: A programming language for software integration and development. *J. Mol. Graphics Modell. 17*, 57–61.
56. Sanner, M. F., Olson, A. J., and Spehner, J. C. (1996) Reduced surface: An efficient way to compute molecular surfaces. *Biopolymers 38*, 305–320.
57. Marion, D., and Wuthrich, K. (1983) Application of phase sensitive two-dimensional correlated spectroscopy (COSY) for measurements of ^{1}H-^{1}H spin-spin coupling constants in proteins. *Biochem. Biophys. Res. Commun. 113*, 967–974.
58. Wüthrich, K. (1986) NMR of Proteins and Nucleic Acids, Wiley-Interscience, New York.
59. Wishart, D. S., Sykes, B. D., and Richards, F. M. (1992) The chemical shift index: A fast and simple method for the assignment of protein secondary structure through NMR spectroscopy. *Biochemistry 31*, 1647–1651.
60. Hutchinson, E. G., and Thornton, J. M. (1996) PROMOTIF: A program to identify and analyze structural motifs in proteins. *Protein Sci. 5*, 212–220.
61. Baldwin, J. M., Schertler, G. F., and Unger, V. M. (1997) An α-carbon template for the transmembrane helices in the rhodopsin family of G-protein-coupled receptors. *J. Mol. Biol. 272*, 144–164.
62. Shim, J. Y., Welsh, W. J., and Howlett, A. C. (2003) Homology model of the CB1 cannabinoid receptor: Sites critical for nonclassical cannabinoid agonist interaction. *Biopolymers 71*, 169–189.
63. Shi, L., Liapakis, G., Xu, R., Guarnieri, F., Ballesteros, J. A., and Javitch, J. A. (2002) *β*2 adrenergic receptor activation. Modulation of the proline kink in transmembrane 6 by a rotamer toggle switch. *J. Biol. Chem. 277*, 40989–40996.
64. Reggio, P. H. (2003) Pharmacophores for ligand recognition and activation/inactivation of the cannabinoid receptors. *Curr. Pharm. Des. 9*, 1607–1633.
65. Meschler, J. P., Kraichely, D. M., Wilken, G. H., and Howlett, A. C. (2000) Inverse agonist properties of N-(piperidin-1-yl)-5-(4-chlorophenyl)-1-(2, 4-dichlorophenyl)-4-methyl-1H-pyrazole-3-carboxamide HCl (SR141716A) and 1-(2-chlorophenyl)-4-cyano-5-(4-methoxyphenyl)-1H-pyrazole-3-carboxylic acid phenylamide (CP-272871) for the CB_1 cannabinoid receptor. *Biochem. Pharmacol. 60*, 1315–1323.
66. Pertwee, R. G. (2005) Inverse agonism and neutral antagonism at cannabinoid CB1 receptors. *Life Sci. 76*, 1307–1324.
67. Sargent, D. F., and Schwyzer, R. (1986) Membrane lipid phase as catalyst for peptide-receptor interactions. *Proc. Natl. Acad. Sci. U.S. A. 83*, 5774–5778.
68. Sankararamakrishnan, R. (2006) Recognition of GPCRs by peptide ligands and membrane compartments theory: Structural studies of endogenous peptide hormones in membrane environment. *Biosci. Rep. 26*, 131–158.
69. Zdobinsky, T., Scherkenbeck, J., Zerbe, O., Antonicek, H., and Chen, H. (2009) Structures of micelle-bound selected insect neuropeptides and analogues: Implications for receptor selection. *ChemBioChem 10*, 2644–2653.
70. Scrima, M., Campiglia, P., Esposito, C., Gomez-Monterrey, I., Novellino, E., and D'Ursi, A. M. (2007) Obestatin conformational features: A strategy to unveil obestatin's biological role? *Biochem. Biophys. Res. Commun. 363*, 500–505.
71. D'Ursi, A. M., Albrizio, S., Di Fenza, A., Crescenzi, O., Carotenuto, A., Picone, D., Novellino, E., and Rovero, P. (2002) Structural studies on Hgr3 orphan receptor ligand prolactin-releasing peptide. *J. Med. Chem. 45*, 5483–5491.
72. Dodd, G. T., Mancini, G., Lutz, B., and Luckman, S. M. (2010) The peptide hemopressin acts through CB1 cannabinoid receptors to reduce food intake in rats and mice. *J. Neurosci. 30*, 7369–7376.